

Title no. 109-M62

Hydraulic Pressure Cracking in Rail Seats of Concrete Crossties

by John C. Zeman, J. Riley Edwards, David A. Lange, and Christopher P. L. Barkan

Rail seat deterioration (RSD) is the deterioration of the crosstie concrete underneath the rail that causes track geometry problems and weakens the track structure. RSD may have up to five potential mechanisms, and this research investigates one of them: hydraulic pressure cracking. A laboratory test apparatus and procedure were devised to measure the surface water pressure in a laboratory rail seat using rail pads of differing material composition and surface geometry. A model of the effective stress in a concrete-crosstie rail seat was developed to estimate the water pressures on the rail seat surface and whether they could lead to damaging pore pressures in the concrete. Comparing the effective stress model and the measured surface water pressures, hydraulic pressure cracking appears to be a feasible mechanism for RSD, given the correct combination of high rail seat loads, sufficient moisture, and a rail pad surface that generates high water pressure.

Keywords: crosstie; effective stress; pore pressure; rail seat deterioration; railroad; railway; sleeper.

INTRODUCTION

Ballasted railway track provides support and stability for train traffic by properly distributing the loads and maintaining the required track geometry (Hay 1982). The role of concrete crossties (referred to as “sleepers” elsewhere in the world) in this system is to support the rails under load, distribute the stresses at the rail seat to acceptable levels for the ballast layer, and, along with the ballast and subgrade, maintain proper geometry of the track structure (White 1984). Concrete railway crossties are prestressed, precast beams (Weber 1969). The rail seats are locations on the crosstie that bear the rails and provide embedded steel inserts (or “shoulders”) for fixation. The assembly that fastens the rail to the crosstie commonly consists of a thermoplastic pad or pad assembly between the concrete rail seat and the base of the rail (referred to as a “rail pad”); cast-in, steel-shoulder inserts; spring clips attached to the shoulder inserts that hold the rail; and plastic insulators between the clips/shoulders and the rail. The design and manufacture of concrete crossties in North America is primarily guided by Part 4 of Chapter 30 of the American Railway Engineering and Maintenance-of-Way Association (AREMA) *Manual for Railway Engineering* (AREMA 2009).

Rail seat deterioration (RSD) is degradation underneath the rail on a concrete crosstie and has been cited by major North American freight railroads as the most critical problem with concrete crosstie service life and performance (Zeman et al. 2009). Based on the North American freight railroads' experience with concrete crossties in service and the results of full-scale testing, heavy axle loads, abrasive fines, moisture, and rail movement appear to be the causes of RSD (Bakharev 1994; Peters and Mattson 2004; Reiff 1995). The deterioration of the concrete may result from multiple mechanisms or physical processes. Industry

opinion and previous studies (Bakharev 1994; Choros et al. 2007; Peters and Mattson 2004) suggest that concrete deterioration in RSD may be due to abrasion, crushing, freezing-and-thawing cracking, hydraulic pressure cracking, hydro-abrasive erosion, or some combination of these mechanisms.

A previous microscopy study concluded that a sample of concrete crossties taken out of service with RSD showed characteristics of abrasion and possibly hydraulic pressure cracking or freezing-and-thawing cracking. Hydraulic pressure cracking is microcracking that results when loads pressurize the surface water at the rail seat, leading to damaging pore pressure (tensile stress) within the concrete (Bakharev 1994). Hydraulic pressure cracking and freezing-and-thawing cracking have similar appearances because they both result from high pore water pressures in the concrete. The study did not find microstructural evidence of hydro-abrasive erosion in the samples, nor did it find evidence that alkali-silica reactivity (ASR) was an active mechanism. In addition to surface wear characterized as abrasion, the sample concrete rail seats had characteristic cracks, described as vertical cracks, reaching as deep as 0.8 in. (20 mm) below the surface and horizontal cracks at depths of 0.2 and 0.6 in. (5 and 15 mm) (Bakharev 1994).

In light of the microscopy findings, Bakharev (1994) evaluated the hydraulic pressure cracking hypothesis with a two-dimensional linear-elastic model combining the compressive wheel stresses and the tensile pore pressure in the concrete. Bakharev (1994) assumed that the surface water pressure at the rail seat was equal to the applied load divided by the rail seat area. The location of stresses predicted by the study's model was consistent with the subsurface cracking observed in the sample crossties showing signs of RSD. The study's model predicted significant tensile stresses in the concrete 2 to 4 in. (50 to 100 mm) below the rail seat surface (Bakharev 1994).

In this study, the potential mechanism of hydraulic pressure cracking was explored with three hypotheses: (A) the surface water pressure beneath a loaded rail pad is directly proportional to the applied load; (B) the surface water pressure varies depending on the sealing characteristics of the rail pad; and (C) the surface water pressure is sufficient to cause microcracking in concrete and contribute to RSD. The first two hypotheses were evaluated with laboratory tests, while the last hypothesis was evaluated by comparing the

ACI Materials Journal, V. 109, No. 6, November-December 2012.

MS No. M-2011-274.R1 received September 21, 2011, and reviewed under Institute publication policies. Copyright © 2012, American Concrete Institute. All rights reserved, including the making of copies unless permission is obtained from the copyright proprietors. Pertinent discussion including author's closure, if any, will be published in the September-October 2013 *ACI Materials Journal* if the discussion is received by June 1, 2013.

John C. Zeman is an Engineer Intern in the Transportation/Structural Engineering Section of Farnsworth Group, Inc., Bloomington, IL. He received his BS and MS in civil engineering from the University of Illinois at Urbana-Champaign (UIUC), Urbana, IL. His research interests include the concrete crosstie problem known as rail seat deterioration.

J. Riley Edwards is a Lecturer in the Rail Transportation and Engineering Center (RailTEC) at UIUC. His research interests include the investigation of concrete crosstie and fastening system failure mechanisms and design improvements, and the use of advanced sensing technologies to enhance the efficiency of current railroad mechanical and track inspection practices.

David A. Lange, FACI, is a Professor of Civil and Environmental Engineering at UIUC. He is a member of the ACI Board of Direction and is Chair of ACI's Technical Activities Committee. He is a member of ACI Committees 236, Material Science of Concrete; 237, Self-Consolidating Concrete; 544, Fiber-Reinforced Concrete; S802, Teaching Methods and Educational Materials; and S803, Faculty Network Coordinating Committee. In 2003, he was awarded the ACI Wason Medal for Most Meritorious Paper.

Christopher P. L. Barkan is a Professor, George Krambles Faculty Fellow, and Director of RailTEC at UIUC. His research interests include railroad safety and risk analysis, accident prevention, railroad energy efficiency, rail line capacity analysis, and development of new rail technologies.

results of the laboratory tests with a linear-elastic effective stress model of the concrete.

RESEARCH SIGNIFICANCE

Prestressed concrete crossties have the potential to withstand heavier axle loads and higher traffic volumes than

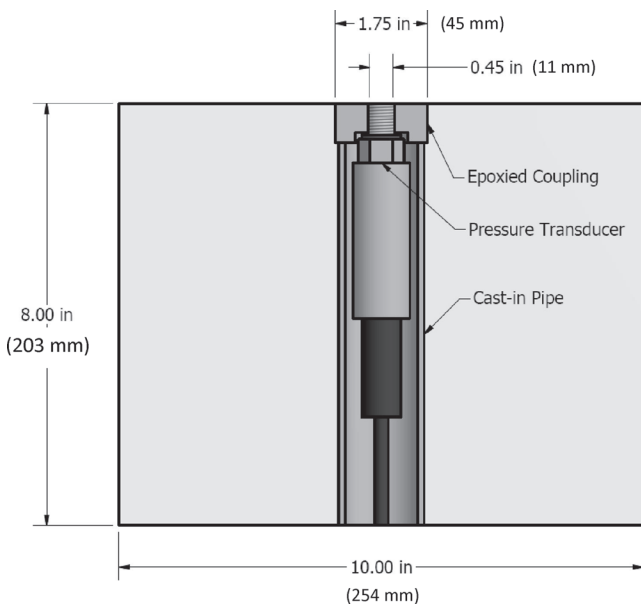


Fig. 1—Cross-section drawing of concrete block with pressure transducer.

Table 1—Concrete block mixture design and average properties

Mixture design		Average properties	
0.75 in. (20 mm) limestone (SSD*)	1809 lb/yd ³ (1074 kg/m ³)	Air content	9.0%
Sand (SSD)	1242 lb/yd ³ (737 kg/m ³)	Slump	2.25 in. (57 mm)
Type III cement	640 lb/yd ³ (380 kg/m ³)	Unit weight	142 lb/ft ³ (2276 kg/m ³)
Water	205 lb/yd ³ (122 kg/m ³)	Compressive strength (28-day)	8129 psi (56.06 MPa)
Air-entraining admixture	23 mL		
High-range water-reducing admixture	192 mL		

*SSD is saturated surface-dry.
Note: 1 mL = 0.034 oz.

other crosstie materials. In addition, high-speed rail (HSR) operations require concrete crossties or slab track because they can maintain the tight geometric tolerances with a stiff track structure and durable, elastic fasteners. Multiple plans for HSR routes in the United States call for HSR passenger trains sharing corridors with heavy-axle-load freight trains. Because North American freight railroads have identified RSD as the most critical problem with concrete crossties (Zeman et al. 2009), RSD also poses a problem for HSR infrastructure in the United States.

EXPERIMENTAL INVESTIGATION

At the Newmark Structural Engineering Laboratory (NSEL) at the University of Illinois at Urbana-Champaign (UIUC), surface water pressure was generated and measured by applying a load on a submerged, mock concrete-crosstie rail seat.

Materials

Concrete blocks (Fig. 1) were cast with a mixture design that is similar to mixture designs currently used by U.S. concrete crosstie manufacturers (Table 1). The blocks were instrumented with a 6000-pounds-per-square-inch-gauge (psig) (41 MPa) submersible pressure transducer. The steel pipe was cast into the concrete block, while the steel coupling, which mates to the pressure transducer, was secured in place with a high-strength, two-part epoxy. To level the bottom surface of the block, it was capped with a sulfur compound, which is commonly used on ASTM C39 cylinders.

Rail pads are thermoplastic pads or assemblies of different materials and are placed between the rail base and the concrete rail seat. Nine rail pads of different materials and surface geometries were analyzed in this study, including three types of pad assemblies. The rail pad surfaces that were tested were flat polyurethane, grooved polyurethane, dimpled polyurethane, flat ethyl-vinyl acetate (EVA), dimpled EVA, dimpled santoprene, a studded pad with a flat plastic bottom (2-part C), a two-part assembly with a flat plastic bottom (2-part B), and a three-part assembly with a flat foam bottom underneath a steel plate (3-part A).

Procedure

The instrumented concrete blocks were submerged in a water tank and secured in place (Fig. 2). A 100 kip (445 kN) MTS servo-hydraulic actuator was used to apply normal loads to the rail pads on top of the instrumented concrete blocks. The applied loads varied from 20 to 60 kips (89 to 267 kN), with 20 kips (89 kN) approximating the static rail seat load under a typical 286 kip (130 metric ton) railcar (Zeman et al. 2010b) and 60 kips (267 kN) representing a high, dynamic rail seat load (AREMA 2009; AAR 2010). Only a normal

force was considered because it was assumed that lateral forces would have little effect on the surface water pressure beneath the rail pad or would reduce this pressure relative to the normal force case.

Over 180 unique scenarios were tested, and at least one replication was conducted per scenario. The tests involved cyclic loading of the concrete block, cycling the load from a minimum of 5 kips (22.24 kN) up to a maximum load, chosen from 20, 30, 40, 50, or 60 kips (89, 134, 178, 223, or 267 kN). The waveform of the load was chosen from trapezoidal wave (ramping at 200 kip/s [890 kN/s]), square wave, or sinusoidal wave (at a frequency of 2 or 4 Hz). The trapezoidal and square wave tests were conducted at a frequency of 0.5 Hz. Other variables were tested, such as the water level in the tank, the alignment of the rail pad indentations relative to the pressure transducer, and modifications of the rail pad surface geometry (for example, filling indentations or cutting shallow slots). For brevity, these other variables will not be discussed in this paper (Zeman 2010).

When running the tests, water was filled to the desired level, the pad under consideration was placed on the block, and the actuator was lowered to a point of contact (arbitrarily defined as 200 lb [890 N] of force) to secure the pad in place. All tests were run for 30 seconds; a 4 Hz test contained 120 cycles, whereas a 0.5 Hz test contained 15 cycles. The data acquisition rate was set at 5 ms. Between trials with no changes in the water level or pad, the pad was secured to the block while the actuator was raised to allow relaxation of the pad and return of any water that had been expelled from the rail seat during the previous trial. This seemed to be an effective method for creating repeatable results.

ANALYTICAL INVESTIGATION

Bakharev (1994) modeled the surface water pressure as the rail seat load divided by the area. Considering Bernoulli's equation for pipe flow without losses, the energy in the water is divided between the pressure energy and the velocity energy (Munson et al. 2006)

$$\text{water energy} = p + \frac{1}{2}\rho v^2 \quad (1)$$

where p is the pressure; v is the velocity; and ρ is the density of water (1.94 slugs/ft³ [1000 kg/m³]) (Munson et al. 2006). Theoretically, the energy in the surface water at the rail seat would be, at most, the energy imparted by the normal stress on the rail seat (with area A)

$$\text{load energy} = \frac{P}{A} \equiv p + \frac{1}{2}\rho v^2 \quad (2)$$

Equation (2) states that the applied load P will pressurize and/or accelerate the water between the rail pad and the rail seat. In reality, all of the load energy might not be transferred through the water, particularly if the water is not evenly distributed over the rail seat. There will also be energy losses to friction, heat, noise, and strain of the pad. Other factors, such as the permeability of the concrete, wetness of the pad surface, and volume losses to the outside, will also play a major role. However, the Bernoulli equation, as presented herein, illustrates the theoretical extremes for pressure and velocity in the cases where there is: 1) a perfect seal between

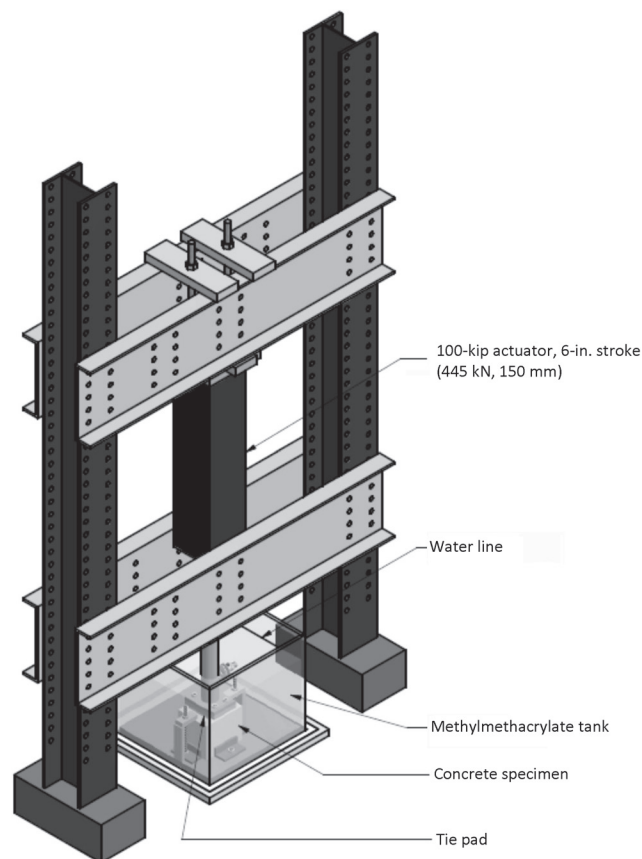


Fig. 2—Isometric drawing of test apparatus.

the rail pad and the rail seat ($v = 0$); 2) no seal ($p = 0$); or 3) an imperfect seal ($p \neq 0, v \neq 0$). Therefore, the surface water pressure will be a direct consequence of the quality of the seal between the pad and the concrete (Zeman et al. 2010c).

Effective stress model

To estimate the pore pressure required to damage the concrete, a linear-elastic model was created to calculate the effective stress beneath the center of the rail seat. This model is an adaptation of an approach developed by Bakharev (1994). The effective stress of the concrete is the total stress—the sum of all the mechanical stresses acting on an element of concrete—minus the pore pressure. With this formulation, stress is taken as positive when it is compressive, and the pore pressure exerts a tensile stress on the concrete, similar to what is experienced by the walls of a pressure vessel. It is the effective stress that must be compared with the concrete's strength to determine if damage will occur.

Considering the effective stress in a concrete cross-section in three dimensions, the total stress state was modeled as the sum of the stress states from a uniform vertical load, a uniform horizontal load, and a prestressed beam on an elastic foundation. These stress contributions were estimated using linear-elastic models to apply superposition. A stress tensor represents the three-dimensional (3-D) state of stress of an infinitesimal element in the form of a 3 x 3 matrix. The diagonals are the normal stresses, while the off-diagonal entries are the shear stresses. By convention, the first, second, and third rows and columns are for the x-, y-, and z-directions, respectively (Hjelmstad 2005). The coordinates used in this model are such that x is parallel

to the axis of the rail, y is parallel to the axis of the crosstie, and z is vertical, positive downward.

To estimate the stress state due to a uniform vertical load, Holl's equations were used, assuming an elastic stress distribution with a Poisson's ratio of 0.5 (Poulos and Davis 1974). The Poisson's ratio of concrete is typically approximately 0.2 (Mindess et al. 2003). The applied normal stress was simply the rail seat load (refer to the Experimental Investigation section for the range of rail seat loads) divided by the rail seat area. At a depth z beneath the center of the rail seat, the stress state due to a uniform vertical load is summarized in the stress tensor S_V , which directly references Holl's equations

$$S_V(z) = 4 \begin{bmatrix} \{\sigma_x\}_V & \{\tau_{xy}\}_V & \{\tau_{xz}\}_V \\ \{\tau_{xy}\}_V & \{\sigma_y\}_V & \{\tau_{yz}\}_V \\ \{\tau_{xz}\}_V & \{\tau_{yz}\}_V & \{\sigma_z\}_V \end{bmatrix} \quad (3)$$

where $\sigma_i \equiv$ normal stress on a face perpendicular to the i -direction, positive when compressive; and $\tau_{ij} \equiv$ shear stress on a face perpendicular to the i -direction, positive in the j -direction.

Similar to the vertical load, the stress state from a uniform horizontal load was estimated with Holl's equations (Poulos and Davis 1974). The uniform horizontal load was estimated by multiplying the uniform vertical load by a lateral-to-vertical load ratio of 0.52 (AREMA 2009). After transforming Holl's stress tensor into the model's coordinate system, the resulting stress tensor S_H (referencing Holl's equations directly) was used

$$S_H(z) = 4 \begin{bmatrix} \{\sigma_y\}_H & -\{\tau_{xy}\}_H & \{\tau_{yz}\}_H \\ -\{\tau_{xy}\}_H & \{\sigma_x\}_H & -\{\tau_{xz}\}_H \\ \{\tau_{yz}\}_H & -\{\tau_{xz}\}_H & \{\sigma_z\}_H \end{bmatrix} \quad (4)$$

For use in the effective stress model, the rail seat shear force and bending moment from a prestressed beam on an elastic foundation model (Zeman et al. 2010a; Zeman 2010) were converted to shear stress and normal stress at different depths, assuming constant (average) shear stress in the section and a linear flexural stress distribution (Craig 2000). By assuming planar bending and an isotropic material, the stress components not on the face of a beam's cross section are unaffected by prestress or flexure (Craig 2000), resulting in the following stress tensor S_B

$$S_B(z) = \begin{bmatrix} 0 & 0 & 0 \\ 0 & \{\sigma_y\}_B & \{\tau_{yz}\}_B \\ 0 & \{\tau_{yz}\}_B & 0 \end{bmatrix} \quad (5)$$

The total stress tensor in the xyz coordinate system is the sum of Eq. (3), (4), and (5)

$$S_{xyz}(z) = S_V(z) + S_H(z) + S_B(z) \quad (6)$$

The total stress tensor was converted to an equivalent principal stress state that is expressed by three mutually perpendicular normal stresses and no shear stress (Hjelmstad 2005). The minimum of these three stresses is referred to as the minor principal stress. It represents the direction in which the concrete is most susceptible to damage from pore pressure. Therefore, the minor principal stress was used to estimate limiting values of pore pressure, which might cause microcracking. By solving the eigenvalue problem for the S_{xyz} tensor, the principal stress tensor is found to be a diagonal matrix of normal stresses, where σ_3 is the minor principal stress

$$S_{123}(z) = \begin{bmatrix} \sigma_1 & 0 & 0 \\ 0 & \sigma_2 & 0 \\ 0 & 0 & \sigma_3 \end{bmatrix} \quad (7)$$

The pore water is assumed to obey Darcy's law, and the concrete is assumed to be fully saturated, such that conservation of mass applies (Bakharev 1994). With these assumptions, the following equation was derived (Zeman 2010) to estimate the pore pressure u at a depth z below the center of the rail seat surface, as a function of the surface water pressure p (A is the surface area of the rail seat, assumed to be square)

$$u = \frac{2p}{\pi} \left[\arctan \left(\frac{\sqrt{A}}{2z} \right) \right] \quad (8)$$

Pascal's law states that a fluid exerts pressure equally to all surfaces that it is contacting, and that these pressures are normal to the contact surfaces (Munson et al. 2006). Therefore, in terms of a stress tensor, the pore pressure can be expressed as equal normal stresses without any shear

$$U(z) = \begin{bmatrix} u & 0 & 0 \\ 0 & u & 0 \\ 0 & 0 & u \end{bmatrix} \quad (9)$$

Then, the effective stress tensor is the result of the principal stress tensor minus the pore pressure tensor, or the difference between Eq. (7) and (9)

$$S'(z) = S_{123}(z) - U(z) = \begin{bmatrix} \sigma_1 - u & 0 & 0 \\ 0 & \sigma_2 - u & 0 \\ 0 & 0 & \sigma_3 - u \end{bmatrix} \quad (10)$$

Damage limits

The resistance of the concrete to spalling due to effective tensile stresses in one direction was simply assumed to be the uniaxial tensile strength of the concrete, which is approximately 10% of the 28-day compressive strength. AREMA (2009) recommends a minimum 28-day compressive strength of 7000 psi (48 MPa). A further simplification

can be made to estimate the fatigue limit for concrete under any kind of action as approximately 50% of the ultimate strength. The actual tensile strength of the concrete is dependent on the stress state and is complicated because this is a triaxial state of stress (Mindess et al. 2003). It is possible that the variability of the actual strength of the concrete would be large enough that considering a complex model of the triaxial tensile strength would not provide a substantially different solution.

Given the recommended minimum strength of 7000 psi (48 MPa) and the stated assumptions, the tensile strength f'_t was approximated as 700 psi (4.8 MPa), while the fatigue limit was approximated as 350 psi (2.4 MPa). These estimated damage limits were imposed on the effective stress, and these relationships were rearranged to put limits in terms of pore pressure as shown

$$\text{To maintain: } \min(S') = \sigma_3 - u \geq \left\{ \begin{array}{l} \frac{1}{2} f'_t \\ f'_t \end{array} \right\} \quad (11)$$

Require:

$$u \leq \left\{ \begin{array}{l} \sigma_3 - \frac{1}{2} f'_t \\ \sigma_3 - f'_t \end{array} \right\} = \left\{ \begin{array}{l} \sigma_3 + (350 \text{ psi [2.4 MPa]}) \\ \sigma_3 + (700 \text{ psi [4.8 MPa]}) \end{array} \right\} = \left\{ \begin{array}{l} u_{\text{fatigue}} \\ u_{\text{strength}} \end{array} \right\} \quad (12)$$

To compare the results of the effective stress model with the empirical surface pressure measurements, the pore pressure limits were converted to surface pressure limits with the following procedure:

1. Choose a discrete value for the applied load (for example, 40 kips [178 kN]) and solve Eq. (3) through (7) and (12) to get u_{fatigue} and u_{strength} .
2. Using Eq. (8), find the minimum surface pressure p such that $u(z) = u_{\text{fatigue}}$ at some depth z to get p_{fatigue} . Likewise, find p_{strength} .
3. Repeat Steps 1 and 2 to get the surface pressure limits for other discrete values of the applied load.

The surface pressure limits from the effective stress model are summarized in Table 2. For these cases of applied load in Table 2, the depth z at which the model predicted the pore pressure would exceed either the fatigue or the strength limit was typically 1 to 2 in. (25 to 50 mm) below the rail seat surface. Bakharev (1994) found microcracks in the sample rail seats originating at approximately the same depth. Based on the characteristics of the cracks, Bakharev (1994) concluded that these microcracks could have been caused by either hydraulic pressure or freezing-and-thawing cycles.

EXPERIMENTAL RESULTS AND DISCUSSION

After plotting the peak surface pressure for each pad versus the applied load (Fig. 3), it was determined that all the tie pads could be organized into one of three groups: flexible (flat and grooved polyurethane, dimpled santoprene); semi-rigid (flat and dimpled EVA, dimpled polyurethane); or assembly with a rigid layer (all three pad assemblies). The pads were placed in these categories solely by their load-pressure behavior, and these names were assigned to the groups in an attempt to explain the differences between them. The mean regression lines that fit the experimental data were plotted on the same graph, sorted by these pad groups (Fig. 3). For the case of a perfect seal, the surface

pressure would be equal to the load divided by the area of the rail seat, and this is plotted in Fig. 3 for comparison, labeled “uniform load stress.”

Both the mean and upper 95% load-pressure models for each of the three rail pad groups, showing the R^2 values and number of trials in each sample, are presented in Table 3. The mean regression lines fit the load-pressure data well for the flexible and semi-rigid pads, with R^2 values of 0.825 and 0.936, respectively (Table 3). This seems to verify Hypothesis (A)—the surface water pressure beneath a loaded rail pad is directly proportional to the applied load—for the flexible and semi-rigid pads. There was significant scatter in the pad assembly data, yielding low R^2 values; however, because the pad assemblies also generated pressures below the predicted damage limits, the variability in their results was not a cause for concern. The load-pressure data plotted in Fig. 3 include data from tests with different waveforms, or loading rates, which were described previously in the Procedure section. The fact that the data still plot with a good linear fit suggests that the loading rate (train speed) does not have a strong influence on the surface pressure.

The most likely source of variation in the test results was the difficulty in controlling the contact angle between the loading plate and the rail seat block. Advancing the actuator with a non-zero contact angle between the loading plate and the block most likely provided the surface water with a path to escape more easily. Without a contact angle, there would be a greater chance that a seal would develop between the pad and the concrete before the surface water could be expelled. This may explain some of the scatter in the recorded peak

Table 2—Surface pressure limits, assuming saturated concrete

	Applied load P					
	kips	20	30	40	50	60
Fatigue limit	psig	580	660	720	770	810
	kPa	4000	4550	4960	5310	5580
Strength limit	psig	945	1090	1180	1260	1320
	kPa	6510	7510	8130	8680	9090

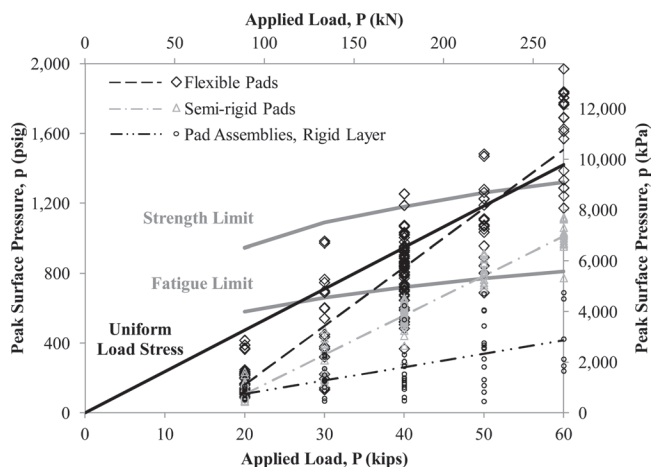


Fig. 3—Peak surface pressure measurements versus applied load, sorted by pad group.

Table 3—Mean and upper 95% regression models for three pad groups

Pad group	Pads	Units	Trend line	R ²	No. of trials
Flexible	Flat polyurethane, grooved polyurethane, dimpled santoprene	p (psig), P (kips)	Mean: $p = 33.7P - 513.9$; Upper 95%: $p = 36.1P - 415.2$	0.825	157
		p (kPa), P (kN)	Mean: $p = 52.2P - 3541$; Upper 95%: $p = 55.9P - 2861$		
Semi-rigid	Dimpled polyurethane, dimpled EVA, flat EVA	p (psig), P (kips)	Mean: $p = 22.7P - 347.8$; Upper 95%: $p = 23.8P - 300.0$	0.936	104
		p (kPa), P (kN)	Mean: $p = 35.1P - 2396$; Upper 95%: $p = 36.8P - 2067$		
Assemblies	2-part B, 2-part C, 3-part A	p (psig), P (kips)	Mean: $p = 7.7P - 46.3$; Upper 95%: $p = 10.5P + 66.6$	0.338	73
		p (kPa), P (kN)	Mean: $p = 11.9P - 319$; Upper 95%: $p = 16.3P + 459$		

surface pressures. The potential implications in track are that rail roll or tilt could lead to similar non-zero contact angles between the rail base and the rail seat. If a non-zero contact angle occurs, it may reduce the actual surface pressure that is generated at the rail seat.

The mean load-pressure model for the flexible pads is close to the ideal uniform load stress (Fig. 3), suggesting that the flexible pads created a nearly perfect seal. Allowing some of the water to escape or flow rather than become pressurized may explain the lower pressures generated with the semi-rigid pads. These results suggest that some tie pads create more effective seals than others, apparently verifying Hypothesis (B)—the surface water pressure varies depending on the sealing characteristics of the rail pad. Differences in material properties and surface geometry may explain the difference in sealing characteristics (Zeman et al. 2010c).

The grooved and flat polyurethane pad surfaces were two sides of the same tie pad. These surfaces generated very similar load-pressure curves. The dimpled and flat EVA pads also generated similar load-pressure curves, despite the difference in surface geometry, suggesting that isolated indentations may not significantly change the load-pressure behavior. It is important to note that the dimpled EVA and flat EVA are dissimilar pads with different thicknesses, providing a slightly different comparison than between the grooved and flat polyurethane. Although the two EVA pads are nominally the same material, there is room for variation of material properties to fit a specific product, similar to how a concrete mixture is adjusted to produce different strengths. The same can be said about the dimpled and flat polyurethane pads, which appear to have slightly different stiffness and hardness properties (Zeman et al. 2010c). The major difference between the dimpled santoprene and the dimpled polyurethane pads is that the santoprene rubber was relatively flexible and compressible and underwent permanent deformation after a few trials. These observations provide evidence that the material properties of the contacting pad partly determined what surface pressures were generated.

The studded pad (the top layer of 2-part C), which was the only pad to have narrow channels running along its full length (providing openings at the pad boundaries), did not generate any measurable pressure in any of its trials. The same results were observed when a dimpled pad and a grooved pad were modified to provide 2 mm (0.08 in.) wide channels from the indentation above the measurement point to the pads' edges. These observations suggest that providing direct flow paths along the contact surface results in an effective absence of a seal under load.

Both the hardest contact surface (the plastic bottom of the two-part assemblies) and the softest contact surface (the foam bottom of the three-part assembly) generated low load-pressure curves (Fig. 3 and Table 3). For the plastic bottoms,

it is possible that it was difficult to create a seal with a relatively hard, stiff material, allowing water to flow rather than becoming pressurized. After one trial (applying up to 120 load cycles), the soft foam bottom would become permanently deformed. During the first trial, the foam apparently created an adequate seal and developed pressure not too far below that of the semi-rigid pads. When a subsequent trial was run with the same pad, a lower pressure was obtained, and even lower pressures were generated with subsequent, higher loads. It may be that the deformation of the foam destroyed its sealing capability and allowed the water to flow. Once the foam deformed and became an ineffective seal, the pressure behavior of the three-part assembly was likely dictated by the hard, rigid metal layer in the middle, which would not readily form a seal.

COMPARISON OF PREDICTIONS AND EXPERIMENTAL RESULTS

The fatigue and strength limits from the effective stress model (Table 2) are plotted in Fig. 3 for comparison with the mean regression models. The flexible pads, on average, exceeded the fatigue limit between 30 and 40 kip (134 and 178 kN) applied load and exceeded the strength limit between 50 and 60 kip (223 and 267 kN) applied load. On the other hand, the semi-rigid pads exceeded the fatigue limit with 50 kip (223 kN) applied load but did not exceed the strength limit within 60 kips (267 kN). Therefore, for rail seat loads above 50 kips (223 kN), there is the potential that a flexible pad could initiate microcracking in the concrete. It is also possible that fatigue damage could result for either flexible or semi-rigid pads if the proper conditions are met and repeated for millions of cycles (Zeman 2010).

In an attempt to evaluate the sensitivity of the surface pressure limits to the various assumptions made when creating the effective stress model, the fatigue limit for various cases was plotted with the mean regression models (Fig. 4), while the strength limit for various cases was plotted with the upper 95% regression models (Fig. 5) (providing 95% confidence that the peak surface pressure will not exceed those regression lines).

The effective stress model assumes that the concrete is saturated, water acts as an incompressible liquid, and the pressure transfer through the pore network occurs instantaneously. In an unsaturated concrete, the pore volume not taken up by water is filled with air, and water pressure is relieved as water flows through the pores. Therefore, the water pressures throughout the specimen are higher and have greater potential to cause damage in a saturated concrete than in an unsaturated concrete. An important question is whether concrete crossties in track can be fully saturated, even just locally at the rail seat. If not, then the effective stress model presented herein would represent a conservative but poten-

tially invalid prediction for concrete damage limits. One way that the unsaturated case could be considered is to set the surface pressure limit equal to the pore pressure limit, rather than considering it at some depth, as was done for the saturated case (Fig. 4 and 5). Considering unsaturated concrete in this manner pushes the strength limit higher than all of the recorded flexible pad pressures, except those at the highest rail seat loads, and the fatigue limit higher than any of the mean semi-rigid pad pressures.

A significant assumption of the current model is that the concrete damage limits are based on 7000 psi (48 MPa) 28-day strength. This is the minimum strength AREMA (2009) recommends for concrete crossties. In reality, U.S. concrete-crosstie manufacturers commonly use mixtures that produce 28-day strengths well above 7000 psi (47 MPa), reaching up to 11,000 psi (76 MPa). If the model was modified with a higher concrete strength of 10,000 psi (69 MPa), the damage limits would increase. This increase was estimated by changing the concrete tensile strength in Eq. (12) to 1000 psi (6.9 MPa) (Fig. 4 and 5). Increasing the concrete strength of the unsaturated case to 10,000 psi (69 MPa) shifts the fatigue limit up to the base case's strength limit, making fatigue damage seem very unlikely, even for the flexible pads.

As mentioned in the Analytical Investigation section, Holl's elastic stress distribution equations were for a Poisson's ratio of 0.5, whereas the Poisson's ratio of concrete is closer to 0.2. This discrepancy between the model and the actual concrete material was accepted because the resulting equations for a 3-D state of stress were readily available. For elastic stress distributions, choosing a larger Poisson's ratio generally results in a stiffer material and thus greater confining stresses than would be observed with a smaller Poisson's ratio (Poulos and Davis 1974). The assumption of modeling concrete as a linear-elastic material could result in higher confining stresses than would be reasonable if the predicted stress in the concrete begins to approach its compressive strength. Depending on the specific concrete in use, the stress-strain curve may exhibit inelastic (nonlinear) strain-softening behavior at moderate-to-high strains, which would result in lower stresses at the same strain (Mindess et al. 2003). The error in these assumptions combined could be as high as 20%, considering other elastic stress distribution models (Poulos and Davis 1974). In an attempt to consider the overestimation of confinement stresses, the minor principal stress term in Eq. (12) was reduced by 20% (Fig. 4 and 5). This consideration did not affect the surface pressure limits significantly.

The previous discussion, along with Fig. 4 and 5, demonstrates how Hypothesis (C)—the surface water pressure is sufficient to cause microcracking in concrete and contribute to RSD—seems to be verified for certain conditions. Conversely, it appears that hydraulic pressure cracking can be effectively mitigated by using a rail pad that does not seal water, minimizing the occurrence of high-dynamic wheel loads, and/or producing concrete crossties with sufficiently high-strength and dense (low-permeability) concrete. When selecting mitigation options, however, the other concrete deterioration mechanisms of RSD must be considered (Zeman et al. 2010c).

SUMMARY AND CONCLUSIONS

Based on the results of the laboratory experiments and the damage limits defined by the effective stress model,

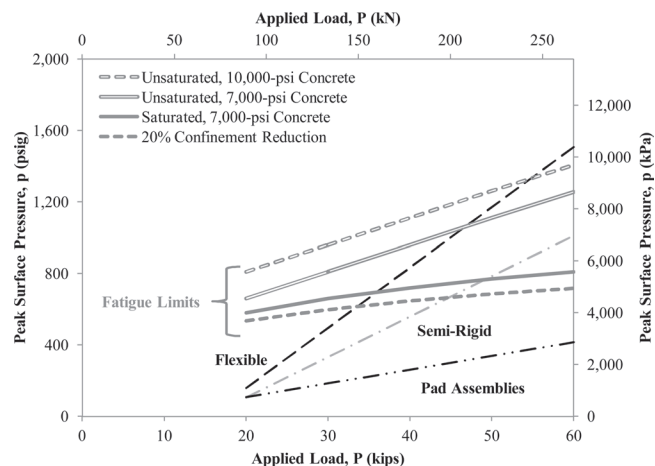


Fig. 4—Sensitivity of fatigue limit compared with mean regression models. (Note: 1 psi = 6.89 kPa.)

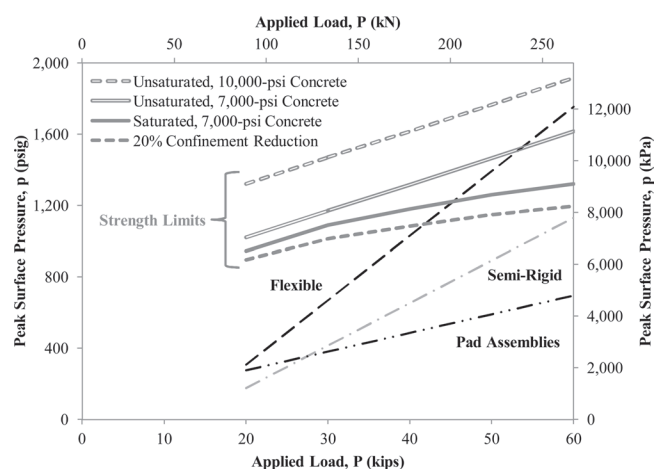


Fig. 5—Sensitivity of strength limit compared with upper 95% regression models. (Note: 1 psi = 6.89 kPa.)

hydraulic pressure cracking appears to have the potential to initiate or contribute to RSD as a concrete deterioration mechanism. The results suggest that this deterioration mechanism can be effectively prevented by implementing one or more of the following approaches: 1) selecting or designing a rail pad that does not seal water and therefore does not generate high surface water pressure; 2) maintaining a low probability of high-impact loads by repairing or removing out-of-round wheels and maintaining uniform load distribution among adjacent crossties; and 3) producing concrete with compressive strength well above the minimum 7000 psi (47 MPa) with proper air entrainment (particularly near the rail seat surface) and low permeability to increase the resistance to cracking, minimize the effects of pore pressure, and reduce the likelihood of saturated concrete beneath the rail seat surface.

The pad assemblies with rigid layers developed little surface pressure at the rail seat. When thermoplastic pads are in contact with the concrete rail seat, it appears that designing the pad with direct escape channels for the water effectively ejects the surface water upon load application rather than pressurizing it. Thermoplastic pads without escape channels created the highest surface pressures, apparently sealing the water during load application. It seems advisable and

relatively simple to incorporate these considerations into future pad and pad assembly designs; however, these design considerations for hydraulic pressure must be balanced with the possibility that allowing water and fines to flow in and out might increase wear due to hydro-abrasive erosion and abrasion (Zeman et al. 2010c).

Based on the linear-elastic effective stress model, these guidelines can make hydraulic pressure cracking an insignificant mechanism. The primary limitations of the effective stress model are the use of linear-elastic constitutive relationships, simple definitions of fatigue and strength crack initiation, and an assumed saturation state of the concrete. Above low levels of strain, concrete typically responds nonlinearly by displaying strain softening until rupture. Accounting for this would result in lower confining stresses and therefore lower resistance to tensile cracking than the current model predicts. A more advanced total stress model would require a nonlinear finite element analysis because superposition could not be employed. Such complex modeling could also result in more realistic predictions of crack initiation and pore pressure distribution. In light of the sensitivity analysis of the damage limits discussed herein, it seems that nonlinear modeling would not produce significantly different conclusions than the linear model.

ACKNOWLEDGMENTS

This project is sponsored by a grant from the Association of American Railroads (AAR) Technology Scanning Program. The authors would like to thank D. Davis and R. Reiff of TTCI; E. Barenberg, G. Banas, and T. Prunkard of the University of Illinois at Urbana-Champaign (UIUC); B. Riehl of RailAmerica Inc.; D. Jackson of Transducers Direct; the AAR Technology Scanning Committee; and the members of AREMA Committee 30—Ties, Subcommittee 4—Concrete Tie Technology, for their invaluable contributions to this research. The authors would also like to acknowledge M. Gutierrez-Romero, R. Kernes, M. Dingler, K. Kilroy, H. Khalil, C. Gross, S. Chadwick, D. Marks, and J. Rudd from UIUC and E. Santana-Santiago of the University of Puerto Rico at Mayaguez for their work on this project. J. C. Zeman has been supported in part by a CN Research Fellowship in Railroad Engineering. J. R. Edwards has been supported in part by grants to the UIUC Railroad Engineering Program from CN, CSX, Hanson Professional Services, Norfolk Southern, and the George Krambles Transportation Scholarship Fund.

REFERENCES

American Railway Engineering and Maintenance-of-Way Association (AREMA), 2009, *AREMA Manual for Railway Engineering*, V. 1, Chapter 30, Parts 2 and 4, American Railway Engineering and Maintenance-of-Way Association, Landover, MD.

- Association of American Railroads (AAR), 2010, *Field Manual of the AAR Interchange Rules*, Association of American Railroads, Washington, DC.
- Bakharev, T., 1994, "Microstructural Features of Railseat Deterioration in Concrete Railroad Ties," MS thesis, University of Illinois at Urbana-Champaign, Urbana, IL.
- Choros, J.; Marquis, B.; and Coltman, M., 2007, "Prevention of Derailments due to Concrete Tie Rail Seat Deterioration," *Proceedings of the ASME/IEEE Joint Rail Conference and the ASME Internal Combustion Engine Division, Spring Technical Conference*, pp. 173-181.
- Craig, R. R., 2000, *Mechanics of Materials*, second edition, John Wiley & Sons, Inc., New York, pp. 81-84.
- Hay, W. W., 1982, *Railroad Engineering*, second edition, John Wiley & Sons, Inc., New York, pp. 239-244, 247-266, 415-416, 469-477, 542-550, 593-597, and 667.
- Hjelmstad, K. D., 2005, *Fundamentals of Structural Mechanics*, second edition, Springer Science + Business Media, LLC, New York, pp. 103-124.
- Mindess, S.; Young, J. F.; and Darwin, D., 2003, *Concrete*, second edition, Pearson Education Inc., Upper Saddle River, NJ, pp. 68-76 and 342-344.
- Munson, B. R.; Young, D. F.; and Okiishi, T. H., 2006, *Fundamentals of Fluid Mechanics*, fifth edition, John Wiley & Sons, Inc., Hoboken, NJ, pp. 39, 402-407, 489-492, and 761.
- Peters, N., and Mattson, S., 2004, "CN 60E Concrete Tie Development," *AREMA Conference Proceedings 2004*, American Railway Engineering and Maintenance-of-Way Association (AREMA), Landover, MD.
- Poulos, H. G., and Davis, E. H., 1974, *Elastic Solutions for Soil and Rock Mechanics*, John Wiley & Sons, Inc., New York, pp. 1-2, 54, 66, and 162-164.
- Reiff, R., 1995, "An Evaluation of Remediation Technologies for Concrete Tie Rail Seat Abrasion in the FAST Environment," *American Railway Engineering Association Bulletin*, V. 96, Bulletin 753, Washington, DC, pp. 406-418.
- Weber, J. W., 1969, "Concrete Crossties in the United States," *PCI Journal*, V. 14, No. 1, pp. 46-57.
- White, J. G., 1984, "Concrete Tie Track System," *Transportation Research Record*, V. 953, pp. 5-11.
- Zeman, J. C., 2010, "Hydraulic Mechanisms of Concrete-Tie Rail Seat Deterioration," MS thesis, University of Illinois at Urbana-Champaign, Urbana, IL.
- Zeman, J. C.; Edwards, J. R.; Barkan, C. P. L.; and Lange, D. A., 2009, "Failure Mode and Effect Analysis of Concrete Ties in North America," *Proceedings of the 9th International Heavy Haul Conference*, Shanghai, China, June, pp. 270-278.
- Zeman, J. C.; Edwards, J. R.; Barkan, C. P. L.; and Lange, D. A., 2010a, "Evaluating the Potential for Damaging Hydraulic Pressure in the Concrete Tie Rail Seat," *Proceedings of the 2010 Joint Rail Conference*, Urbana, IL, Apr.
- Zeman, J. C.; Edwards, J. R.; Barkan, C. P. L.; and Lange, D. A., 2010b, "Investigation of Potential Concrete Tie Rail Seat Deterioration Mechanisms: Cavitation Erosion and Hydraulic Pressure Cracking," *Proceedings of the Transportation Research Board 89th Annual Meeting*, Washington, DC, Jan.
- Zeman, J. C.; Edwards, J. R.; Barkan, C. P. L.; and Lange, D. A., 2010c, "Sealing Characteristics of Tie Pads on Concrete Crossties," *AREMA Conference Proceedings 2010*, American Railway Engineering and Maintenance-of-Way Association (AREMA), Landover, MD.